EUROPEAN ORGANISATION FOR NUCLEAR RESEARCH

ATLAS Internal Note
December 1998

Non-Linear MDT Drift Gases like Ar/CO_2

M. Aleksa[1], W. Riegler[2]

Abstract

Detailed measurements and simulations have been performed, investigating the properties of Ar/CO_2 mixtures as a MDT drift gas. This note presents these measurements and compares them to other drift gases that have been simulated using GARFIELD [1], HEED [2] and MAGBOLTZ [3].
This note also describes systematic errors to be considered in the operation of precision drift chambers using such gases. In particular we analyze effects of background rate variations, gas-density changes, variations of the gas composition, autocalibration, magnetic field differences and non-concentricity of the wire. Their impact on the reconstructed muon momentum resolution was simulated with DICE/ATRECON [4]. The different properties of linear and non-linear drift gases and their relative advantages and disadvantages are discussed in detail.

[1]CERN
[2]Harvard University

Contents

1 Introduction

The gas choice is one of the most critical issues for the muon MDT system. Many different aspects have to be considered. All gases have to fulfil the requirements listed below (see for example [5]):

- Resolution:
  The resolution of one single MDT has to be better than 80 μm. This upper limit is necessary to achieve a muon momentum resolution of $\sim 10\,\%$ for muons with a transverse momentum of $p_T = 1\,\mathrm{TeV/c}$. It is shown in this note, that Ar/CO_2 mixtures have an average resolution of $\sim 50\,\mu$m without background rate (with time slewing correction) and stay below the 80 μm-limit for the highest expected background rates (1500 Hz/cm including an uncertainty factor of 5 for safety).

- Efficiency:
  The efficiency of one MDT without background rate has to be at least 99 %. This requirement is fulfilled by most of the drift gases at a gas pressure of 3 bar and a threshold of $\sim$ 20 primary ionization electrons. For high background rates – we expect count rates of up to 300 kHz per tube (including an uncertainty factor of 5 for safety) – the occupation time of the drift tubes becomes important. A maximum drift time of $t_{max} \approx 700\,\mathrm{ns}$ (baseline gas Ar/CO_2 93/7) translates into an occupancy of 15 %. This is the main reason why fast drift gases are preferred. Measurements and simulations determining the maximum drift time are presented in this note.

- Aging, linearity of the rt-relation:
  Operating at a gas gain of $G_0 = 2 \cdot 10^4$ (baseline) the charge deposit will be 0.6 C/cm in 10 years ATLAS operation. Many drift gases show aging (decrease of the pulse height, high count rates) when being exposed to such conditions. It has been found in extensive aging studies that gas mixtures containing organic compounds (e.g. CH_4) produce thin deposits on the wire and on the cathode which affect the performance (aging). Up to now no linear drift gas (the drift velocity depends only weakly on the electric field) without organic compounds has been found, although some gases with CF_4 come close. The baseline gas (Ar/CO_2 93/7) shows no aging but is rather non-linear. In this note consequences of this non-linearity are investigated and the influence on the spectrometer performance is studied in detail.

- B-field dependence:
  The B-field dependence of the rt-relation should be as small as possible (i.e. small Lorentz angle). In this respect slower drift gases (small Lorentz angle) are preferred. This note shows simulations of the resolution and the systematic error to the rt-relation for the baseline gas (Ar/CO_2 93/7).

- Afterpulsing behavior:
  Afterpulses are a sign for incomplete quenching behavior of the considered gas. Therefore the afterpulsing rate has to be as low as possible. The afterpulsing behavior for several Ar/CO_2 mixtures was measured and is presented in this note.

- Streamer rate:
  The streamer rate has to be smaller than 1 %. Measurements for Ar/CO_2 80/20 showed that it is smaller than 0.5 % for gas gains up to $4 \cdot 10^4$. For Ar/CO_2 93/7 it has not been measured yet.

This note discusses measurements from the testbeam and simulations for several Ar/CO_2 mixtures and compares them to simulations of other drift gases. It analyzes the systematic errors to the rt-relation, and shows an analytical model which can predict these errors. Hence corrections are introduced and tested on testbeam measurements.

2 Working Point Measurements and Simulations

The measurements described in this chapter were performed in the Gamma Irradiation Facility (GIF) in the SPS beam line X5.

They were compared to simulations performed with GARFIELD[1] [1] which is interfaced to HEED[2] [2] and MAGBOLTZ[3] [3].

2.1 Experimental Setup and Rate Environment

The common gamma irradiation test facility of the ATLAS and CMS groups has a 100 GeV muon beam and a ^{137}Cs source with an activity of 740 GBq emitting 662 keV Gammas, which deposit on average an energy of about 36 keV in our MDT's, simulating well the photon background in ATLAS. The actual gamma rate can be adjusted by choosing an appropriate combination of several lead filters.

These measurements were designed to show the gas properties of Ar/CO_2 mixtures, hence only the space charge effects of resolution deterioration (gain drop and field variations, see [6]) were investigated. In order to minimize the electronics effects of resolution deterioration (baseline shift and baseline fluctuations, see [6]) the total count rate per tube was kept low by shielding the entire tube with lead blocks apart from ~ 10 cm around the beam line.

For our investigations the BNL tubes equipped with BNL preamplifiers and shaping amplifiers [7] were used. The shaping amplifiers were adjusted to give maximum undershoot in order to minimize baseline fluctuations. This shaping scheme was discussed as unipolar shaping with undershoot in [6]. Figure 1 shows the readout chain. A FADC and a TDC were read out for each tube. The discriminator threshold was set to 20 electrons.

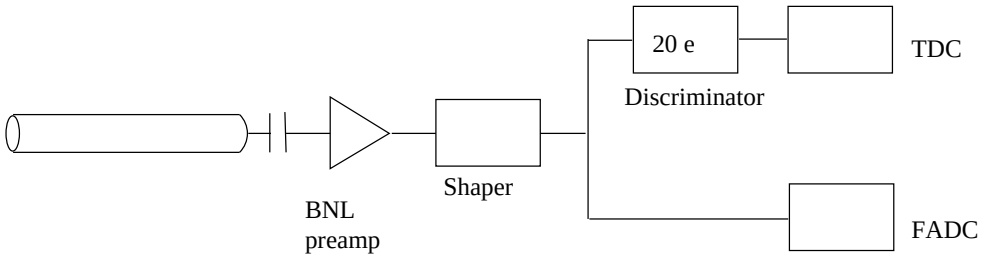

Figure 1: *The readout chain of the tubes analysed in this study.*

The tubes were operated with different Ar/CO_2 mixtures (Ar/CO_2 90/10, Ar/CO_2 92/8, Ar/CO_2 93/7, Ar/CO_2 94/6). The gas mixing facility used digital flow meters with an error of $\sim 0.5\,\%$. This corresponds to an error of smaller than $0.1\,\%$ absolute in the final

[1]Program for simulation of two and three dimensional drift chambers.
[2]Computes in detail the energy loss of fast charged particles in gases.
[3]Computes electron transport parameters for a large variety of gases.

gas mixture (Ar/CO_2 93/7 $\rightarrow$ Ar/CO_2 93.07/6.93 or Ar/CO_2 92.93/7.07). A pressure of 3 bar was applied and gas gains of $2 \cdot 10^4$ and $4 \cdot 10^4$ were used.

The external reference system was ODYSSEUS [8], a beam telescope consisting of 6 Silicon micro-strip detectors with 7 μm resolution each. 4 out of the 6 planes measure the precision coordinate perpendicular to the MDT wires, the other 2 detectors give us the second coordinate parallel to the wires. By extrapolation of the silicon telescope track to the tube position we get a prediction accuracy of 10 μm.

The rates per unit tube length for different lead filters are listed in the table below:

nominal filter factor	rate per unit tube length (Hz/cm)
2	3060
5	1400
10	810

Measurements without background rate and with the rates mentioned above have been performed.

2.2 Gas Gain Measurement

This section shows briefly the results of the gas gain measurements. Only a relative measurement was performed, therefore the systematic error of the gas gain is estimated to be about 20 %. As a reference gas $Ar/N_2/CH_4$ 91/4/5 was used (see [9]). The spectra of a ^{55}Fe source, emitting 5.9 keV photons, were compared and hence the gas gain calibrated.

Figure 2 shows the gas gains for different Ar/CO_2 mixtures at 3 bar gas pressure, a temperature of $\sim$ 295 K, a wire radius $a = 25\,\mu$m and a tube radius $b = 1.46$ cm. Using Diethorn's formula [10] the gas gains for other gas pressures or even other geometries can be calculated ($E(a)$ is the electrical field on the wire, $E_{min}(\rho_0)$ and ΔV are the Diethorn parameters, see table 1):

$$G = \left[\frac{E(a)\rho_0}{E_{min}(\rho_0)\rho_{gas}} \right]^{\frac{aE(a)\log 2}{\Delta V}} \tag{1}$$

gas mixture	E_{min}(1 bar) (kV/cm)	ΔV (V)
Ar/CO_2 80/20	22	49
Ar/CO_2 90/10	20	43
Ar/CO_2 92/8	19	42
Ar/CO_2 93/7	24	34
Ar/CO_2 94/6	23	34

Table 1: *Diethorn parameters E_{min} and ΔV for different Ar/CO_2 mixtures. The errors are about 10 %.*

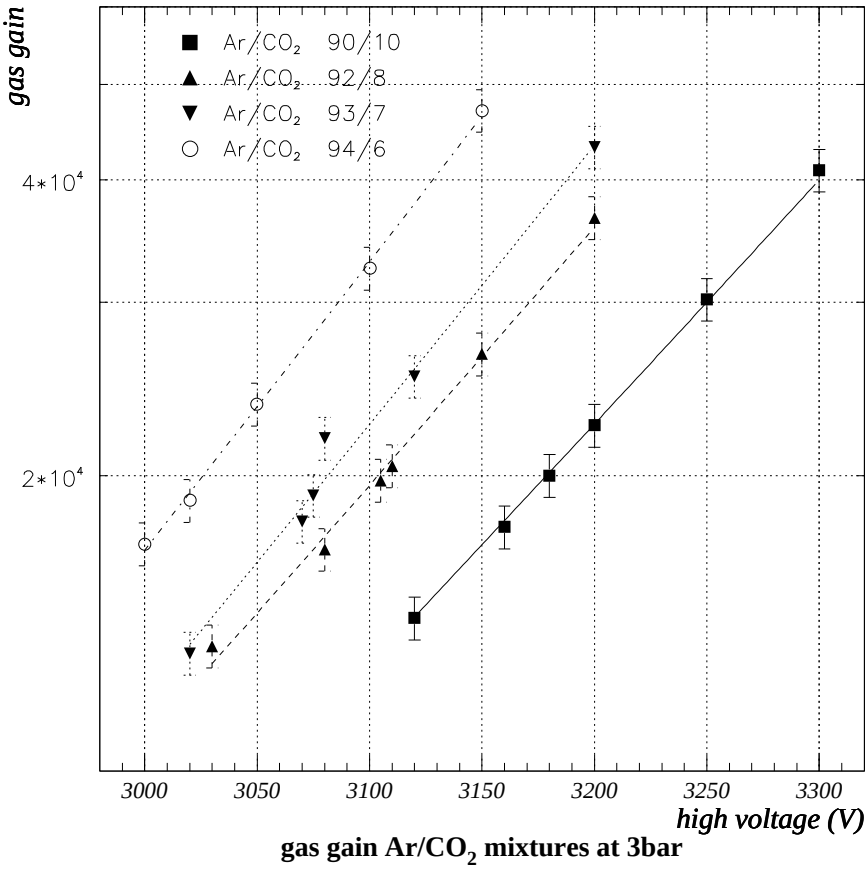

Figure 2: *Gas gains for different Ar/CO_2 mixtures. The Diethorn parameters resulting from the fits are listed in table 1. Note that the plot shows only the statistical errors, the systematic errors due to the relative measurement are estimated to be about 20 %.*

2.3 Afterpulsing

In the avalanche process next to the wire surface UV photons are generated. If such photons reach the conducting cathode free electrons can be created by the photoelectric effect. These electrons will drift towards the wire, multiply and induce a – usually small – signal, which we call afterpulse. Hence these signals are expected to be separated in time from the first avalanche by at least the maximum drift time. Organic molecules, with their many degrees of freedom, have large photo-absorption coefficients over a range of wavelengths that is wider than that for noble gases. Thus they can be used as quench gases. Common quench gases are CH_4 and other hydrocarbons but also inorganic molecules like CO_2.

The afterpulsing rate is a number which quantifies whether a drift gas has a sufficient amount of quenching molecules. In order to distinguish between multiple hits and real

afterpulses only signal pulses were taken into account which showed no hit between the first threshold-crossing time and the time where afterpulses were expected. Figure 3 (a) shows the principle. Dividing the number of entries around the maximum drift time by the number of first threshold crossings yields the afterpulsing rate which is plotted in figure 3 (b) for different CO_2 contents in Ar/CO_2 mixtures.

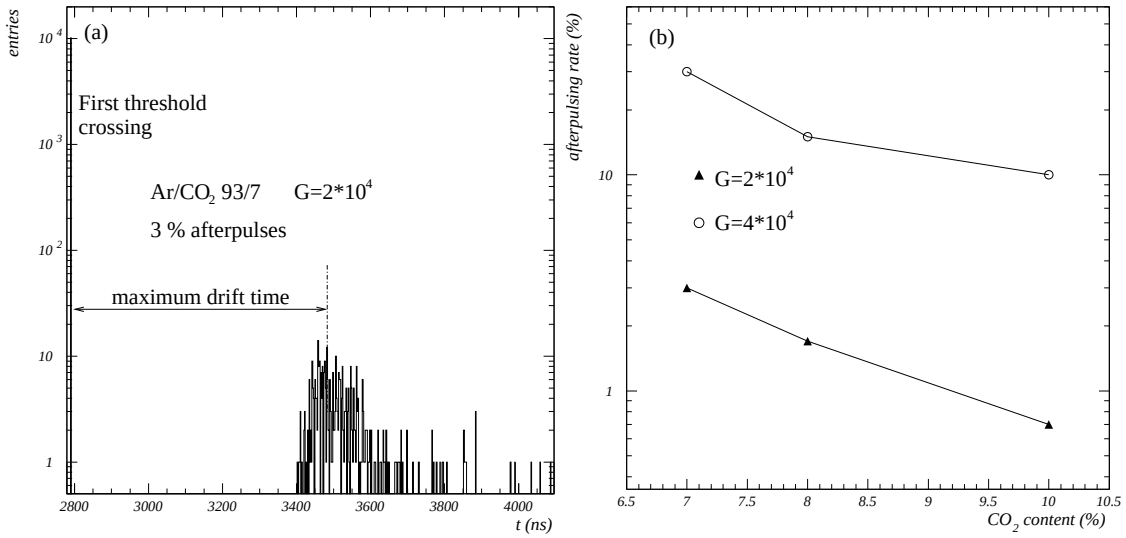

Figure 3: *Afterpulsing rate. (a) shows how the afterpulsing rate was determined: All hits around and after the maximum drift time (3400 ns – 4200 ns, 20 electron threshold) were divided by the number of first threshold crossings. Plot (b) shows the dependence of the afterpulsing rate on the CO_2 content in Ar/CO_2 mixtures. With the same method we got 0.25 % afterpulsing rate for $Ar/N_2/CH_4$ 91/4/5 at a gas gain of $G = 2 \cdot 10^4$.*

Afterpulses produce additional hits but compared to the large uncertainties of the background rate (safety factor 5), they are negligible. Furthermore afterpulses hardly contribute to the occupancy, because they are very short. However, afterpulses are a sign for incomplete quenching properties of a gas which might cause other problems (e.g. higher probability of discharges on damaged wires). The ATLAS muon system will be able to cope with an afterpulsing rate of a few percent. Consequently afterpulses themselves in Ar/CO_2 are no problem at a gas gain of $G = 2 \cdot 10^4$. Nevertheless, for running with higher gas gains additional quench gases will have to be added.

2.4 Hit Multiplicity

Multiple hits per signal can cause readout occupancy and tracking[4] problems. Since the hit multiplicity strongly depends on the drift gas, it is necessary to check how the electronics shaping scheme has to be adjusted to deliver only one hit per signal. This has been studied extensively and is described in [11].

[4]The information whether a hit corresponds to a leading edge of a muon signal is lost.

Due to the longer drift time (Ar/CO_2 93/7: $t_{max} \approx 700\,ns$) and the non-linearity of the rt-relation the hit multiplicity in Ar/CO_2 increases compared to faster, linear gases (e.g. $Ar/N_2/CH_4$ 91/4/5: $t_{max} \approx 485\,ns$).

To compensate this behaviour and to achieve only one hit per signal for gases like Ar/CO_2 93/7, the tail cancellation has to be "soft"[5]. Consequently the trailing edge resolution deteriorates significantly and the dead-time increases slightly. Furthermore a big hysteresis is needed to achieve one single hit per signal. Figure 4 shows the hit multiplicity for two gases as a function of the threshold and the shaping. It can be seen that "soft" tail cancellation and large hysteresis results in 1 hit per signal.

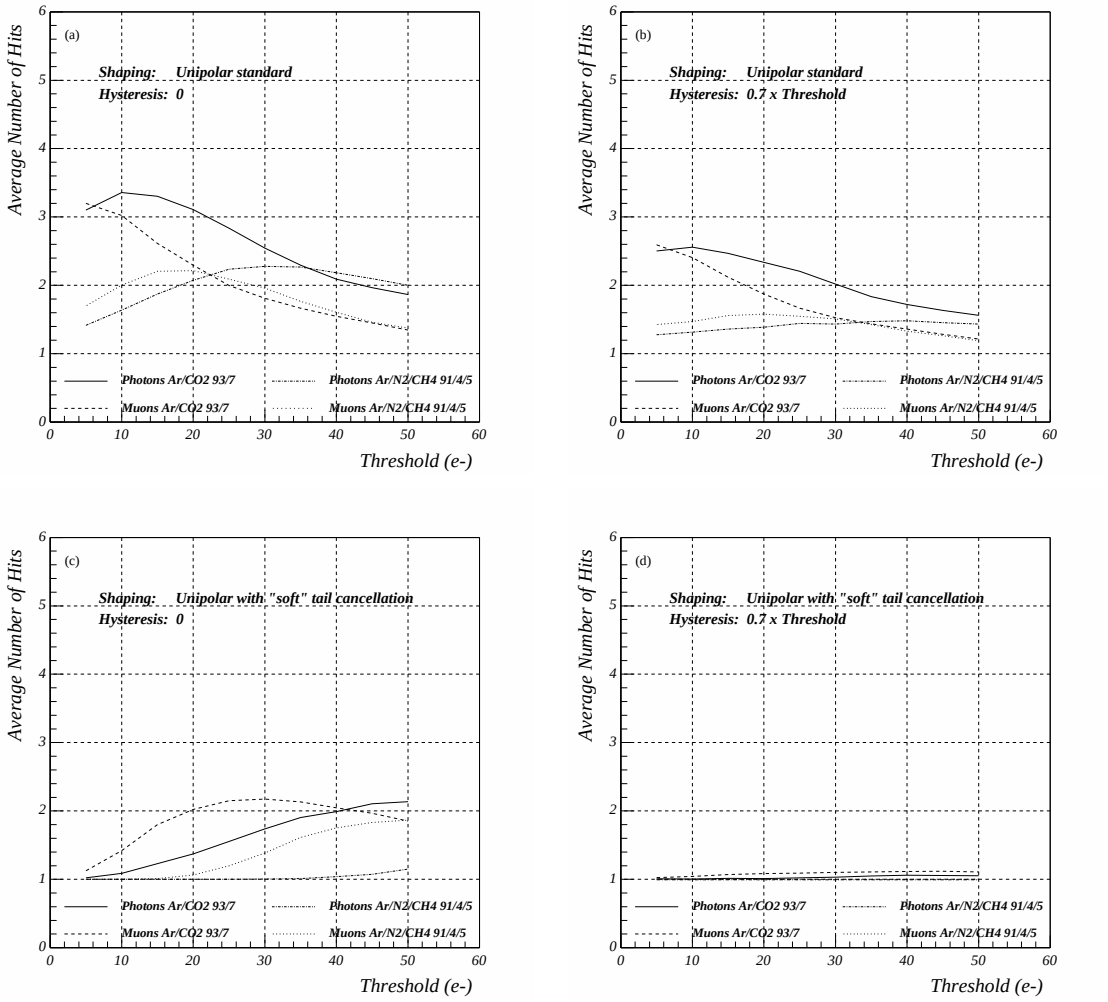

Figure 4: *Hit multiplicity as a function of the threshold for unipolar shaping [11]. The figure compares Ar/CO_2 93/7 with $Ar/N_2/CH_4$ 91/4/5. Shown are GARFIELD simulations for a tube length of $l = 5$ m. Plots (a) and (b) show the hit multiplicity for the standard unipolar shaping, (c) and (d) for unipolar shaping with a "soft" tail cancellation. We see that "soft" tail cancellation and large hysteresis result in a single hit per signal.*

[5]I.e. the long ion tail of the signal is not cancelled entirely.

2.5 Space-Time Relation

Figure 5 shows the rt-relations for several gas mixtures. The Ar/CO_2 mixtures are non-linear, i.e. the drift velocity changes with different electric fields ($E(r) \propto \frac{1}{r}$). Those gases are therefore far more sensitive to variations of the environmental parameters and hence cause systematic errors in the track position (see section 3). For gas mixtures containing CH_4 the drift velocity is almost independent of the electric field. Changes of the drift field due to space charge have hardly any impact, hence the resolution stays unchanged even for high background rates (see section 2.6). So far, no linear gas without CH_4 has been found, although some gases containing CF_4 come close.

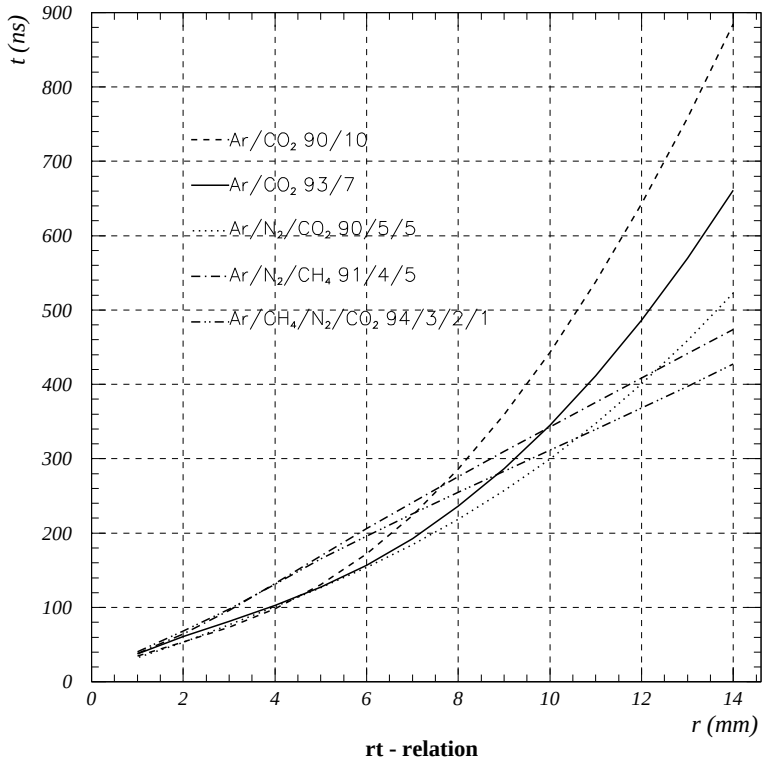

Figure 5: *Space-time relations for different gas mixtures at a gas gain of* $G = 2 \cdot 10^4$ *and a gas pressure of 3 bar.*

2.6 Resolution Studies

The spatial resolution as a function of the drift distance r is defined as the width of the residual distribution as a function of r, which is obtained by comparing the track position r predicted by the reference system (ODYSSEUS) and the track position measured with the drift tube.

The spatial resolution was measured for Ar/CO_2 92/8, Ar/CO_2 93/7 and Ar/CO_2 94/6. The σ_{noise} was 3.8 primary ionization electrons, the threshold was 20 primary ionization electrons, which was approximately 5 times noise. Figure 6 compares the drift-radius dependence of the spatial resolution with GARFIELD simulations [1]. A detailed description

of the way these simulations were done can be found in [6]. Simulations and measurements show excellent agreement. The main effect of resolution deterioration for Ar/CO_2 mixtures – and for other non-linear gases – are the field variations (see [6]). Plot 6 (b) shows the simulated resolution for $Ar/N_2/CH_4$ 91/4/5. This linear drift gas shows only a very small resolution deterioration even at high background rates; the deterioration is mainly caused by the gain drop.

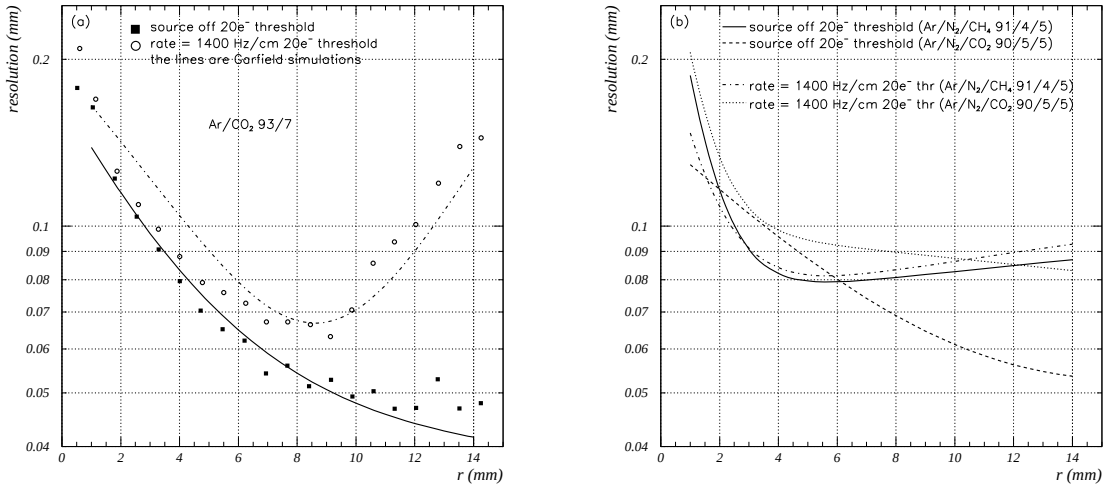

Figure 6: *Spatial resolution as a function of the drift distance ($G_0 = 2 \cdot 10^4$). Plot (a) shows the measurement for the Ar/CO_2 93/7 mixture. The shape of the resolution curve is very similar for all Ar/CO_2 mixtures. Plot (b) shows GARFIELD simulations [1] for $Ar/N_2/CH_4$ 91/4/5 (see also [6]) and $Ar/N_2/CO_2$ 90/5/5. The rate effect for the linear gas in (b) ($Ar/N_2/CH_4$ 91/4/5) is much smaller, nevertheless the resolution ends up at approximately the same level at 1400 Hz/cm (see table 2).*

The average tube resolution is given by quadratically averaging the resolution as a function of r. However, we are more interested in the resolution for a track fit, for which hits are weighted by $\frac{1}{\sigma(r)^2}$. Hence a better figure of merit for our purposes is $\bar{\sigma}$, the inverse quadratic average (IQA), defined by (b is the inner tube radius):

$$\bar{\sigma} = \frac{1}{\sqrt{\left\langle \frac{1}{\sigma^2} \right\rangle}} \qquad \text{with} \qquad \left\langle \frac{1}{\sigma^2} \right\rangle = \frac{1}{b} \int_0^b \frac{1}{\sigma^2(r)}\, dr \quad . \tag{2}$$

Figure 7 shows $\bar{\sigma}$ as a function of rate for different Ar/CO_2 mixtures. The highest expected background rates in ATLAS including a safety factor 5 are 1500 Hz/cm. The measurements presented in the plots go far beyond this rate. Figure 7 (d) gives evidence that the resolution deterioration at a gas gain of $4 \cdot 10^4$ is more severe than for the lower gas gain because of almost twice the amount of space charge[6] being produced in the drift volume. For

[6]Because of the higher gain drop for higher gas gains the amount of space charge does not increase linearly.

the higher gas gain the time slewing correction is rather ineffective since the time slewing contribution to the resolution is already quite small.

The squares in (a), (b), and (c) are resolution measurements using leading edge charge corrections. The integral over the first 20 ns of the signal (i.e. the leading edge) was used to correct for time slewing (see [6] for more details). As expected the method has the bigger effect the faster the gas is: Time slewing introduces a jitter on the threshold crossing time, which has a bigger effect for faster gases. Thus the correction becomes more effective with faster gas mixtures. It can be seen that the small resolution deterioration due to the lower gas gain is completely compensated by the time slewing correction.

In table 2 the values of $\bar{\sigma}$ for different gas mixtures are listed. For low background rates the Ar/CO_2 mixtures have a very much better resolution than linear gases. Even at the highest background rates Ar/CO_2 mixtures still have better resolution.

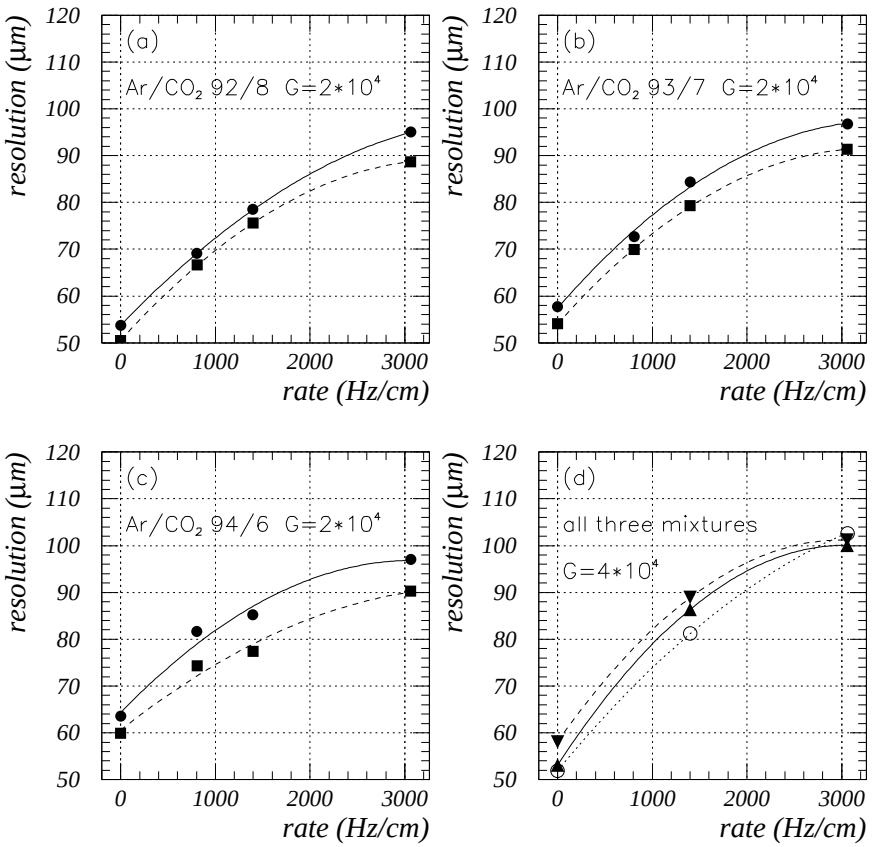

Figure 7: *Spatial resolution (IQA) as a function of rate. The lines are plotted to guide the eyes. Plots (a), (b) and (c) show the spatial resolution of three different Ar/CO_2 mixtures at a gas gain of $G_0 = 2 \cdot 10^4$. The squares show the resolution with leading edge charge correction. Plot (d) shows the resolution versus rate of all three mixtures at a gas gain of $G_0 = 4 \cdot 10^4$.*

gas mixture	$\bar{\sigma}(0\,\mathrm{Hz/cm})$ (μm)	$\bar{\sigma}(1400\,\mathrm{Hz/cm})$ (μm)	t_{max} (ns)
$Ar/N_2/CH_4$ 91/4/5 *	85.6	87.7	485
$Ar/N_2/CO_2$ 90/5/5 *	69.0	93.3	560
$Ar/CH_4/N_2/CO_2$ 94/3/2/1 *	91.9	94.5	440
Ar/CO_2 90/10 *	48.3	78.6	950
Ar/CO_2 92/8	53.7	78.5	770
Ar/CO_2 93/7	57.8	84.3	700
Ar/CO_2 94/6	63.5	85.1	630

Table 2: *Resolution $\bar{\sigma}$ (IQA) and maximum drift time t_{max} for different gas mixtures. The gases marked with * were only simulated. For all measurements and simulations the σ_{noise} was 3.8 primary ionization electrons, the threshold was at 20 primary ionization electrons and the gas gain was $G_0 = 2 \cdot 10^4$. The time slewing correction was not applied.*

2.7 Impact of a Magnetic Field

With a magnetic field B parallel to the wire, the electrons do not travel on radial approach lines towards the wire, but under an angle Ψ (i.e. the Lorentz angle) which is approximately given by

$$\tan\Psi = \frac{eB}{m}\tau, \tag{3}$$

where $\frac{eB}{m}$ is the cyclotron frequency and τ is the mean time between collisions of the electrons with the gas molecules. Consequently the drift time t for a certain drift distance r will increase.

In order to understand the properties of Ar/CO_2 93/7 in the presence of a magnetic field parallel to the wire, GARFIELD simulations[7] with a magnetic field of $B = 0.5\,\mathrm{T}$ ($G = 2 \cdot 10^4$, $p = 3\,\mathrm{bar}$) have been done. Figure 8 (a) shows measurements [12] and MAGBOLTZ [3] simulations of the Lorentz angle Ψ for Ar/CO_2 90/10 at a pressure $p = 1.02\,\mathrm{atm}$ in order to evaluate the validity of the simulations. It can be seen that the simulation yields a very good estimate of the effect of the magnetic field B. Plot 8 (b) presents simulations of the Lorentz angle Ψ for several gases as a function of the radius r.

The following points have been found for Ar/CO_2 93/7:

- the Lorentz angle is $\langle\Psi^{0.5\,\mathrm{T}}\rangle = 9.3\,^\circ$ which is small compared to other gases,
- the maximum drift time t_{max} increases only slightly to $t_{max}^{0.5\,\mathrm{T}} \approx 720\,\mathrm{ns}$ ($t_{max}^{0\,\mathrm{T}} \approx 700\,\mathrm{ns}$ without magnetic field),
- the resolution without background rate remains almost unchanged or improves slightly due to the decreased drift velocity ($\bar{\sigma}^{0.5\,\mathrm{T}} = 56.9\,\mu\mathrm{m}$ instead of $\bar{\sigma}^{0\,\mathrm{T}} = 57.8\,\mu\mathrm{m}$ without magnetic field, both values without time slewing correction,

[7]The transport properties in the presence of a magnetic field B were simulated with MAGBOLTZ [3]

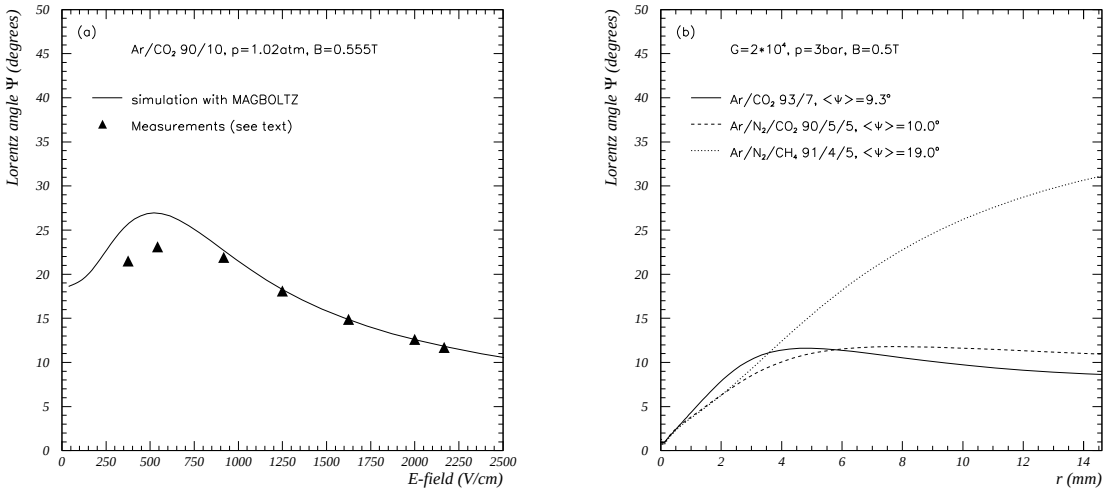

Figure 8: *Lorentz angle. Plot (a) compares MAGBOLTZ [3] simulations with measurements [12]. Plot (b) shows simulations of* Ψ *as a function of the drift radius r for three different drift gases.*

- The high rate behaviour is not influenced by a magnetic field of this strength; i.e. the high rate deterioration of the resolution stays the same ($\bar{\sigma}^{0.5\,\mathrm{T}} = 83.8\,\mu$m for 1400 Hz/cm without time slewing correction).

For the other simulated gases the impact of a magnetic field was higher (see figure 8 (b)).

3 Systematic Errors to the Space-Time Relation

The drift velocity v_D is a function of $\frac{E}{\rho}$. Hence environmental changes which influence either the electric field E or the gas density ρ affect the drift velocity in a tube and consequently the rt-relation. However this effect is negligible for linear gas mixtures (e.g. $Ar/N_2/CH_4$ 91/4/5) because their drift velocity depends only weakly on the ratio of $\frac{E}{\rho}$. For non-linear gas mixtures (e.g. Ar/CO_2 mixtures) these effects become more important. This chapter describes in detail all different effects contributing to systematic errors to the rt-relation.

Variations of the rt-relation during autocalibration will show up as a single tube resolution deterioration and produce perhaps non-Gaussian tails. Changes in the environmental parameters after autocalibration will distort the rt-relation systematically resulting in a wrong prediction of the radius r at a given drift time t. Therefore this chapter deals with the stability of the important parameters. Only considerable changes in time will cause a systematic error to the rt-relation and hence deteriorate the reconstructed muon momentum resolution.

This chapter will describe all effects causing systematic errors to the rt-relation, estimate its influences on the reconstructed muon momentum resolution and finally introduce possible first order corrections to systematic effects.

Different effects will cause deviations from the original rt-relation $r_0(t)$, resulting in

$$r(t) = r_0(t) + \delta r(t). \tag{4}$$

The deviation $\delta r(t)$ and hence $r(t)$ will be functions of the background rate, the gas gain, the gas density, the gas composition, the non-concentricity of the anode wire and the magnetic field. In addition we expect a rather small contribution from the autocalibration itself. Thus we will decompose $\delta r(t)$ into

$$\delta r(t) = \delta r_F(t) + \delta r_G(t) + \delta r_D(t) + \delta r_{gas\,comp}(t) + \delta r_C(t) + \delta r_M(t) + \delta r_{autocal}(t), \tag{5}$$

where $\delta r_F(t)$ is the error due to high background rate induced changes of the drift field (space charge effect), $\delta r_G(t)$ the contribution of the gain drop (space charge effect and temperature effect), $\delta r_D(t)$ the gas density effect (e.g. due to temperature changes), $\delta r_{gas\,comp}(t)$ the expected effect as a consequence of variations in the gas composition, $\delta r_C(t)$ the error due to a non-concentricity of the anode wire, $\delta r_M(t)$ the systematics due to differences in the magnetic field and $\delta r_{autocal}(t)$ the systematic error of the rt-relation obtained by autocalibration.

In the following we will quantify the systematic error to the rt-relation with the root mean square of the difference $\delta r^{\text{r.m.s.}}$ between the original and the distorted rt-relation (a and b are the wire respectively the tube radius):

$$\delta r^{\text{r.m.s.}} = \sqrt{\frac{1}{b}\int_0^b \delta r(r)^2 \, \mathrm{d}r}. \tag{6}$$

3.1 ATLAS Environment

This chapter describes the environment in which the ATLAS muon system is expected to work. Varying background rate, gas density or gas composition cause systematic errors to the rt-relation. Furthermore systematic errors of the rt-relation due to autocalibration, magnetic field differences and non-concentricity of the wire are considered.

3.1.1 Rate Environment

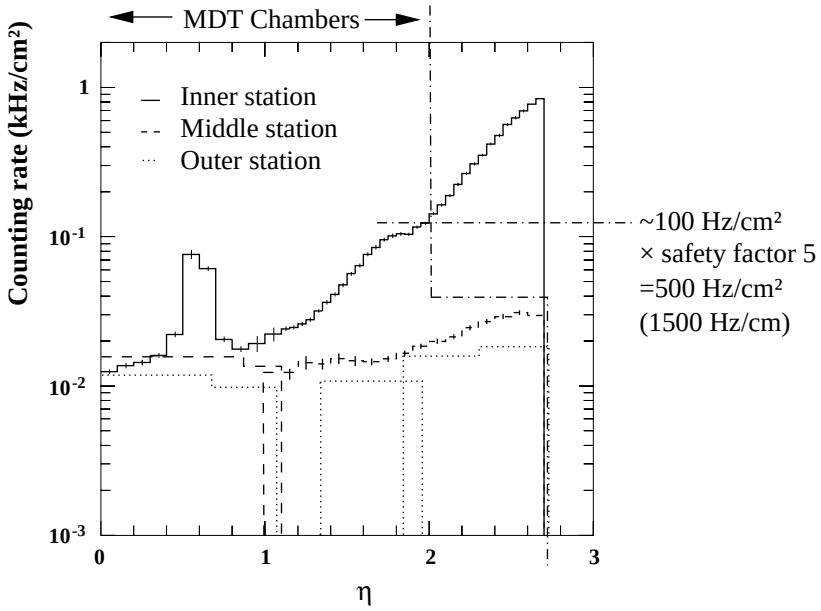

Figure 9: *Pseudo-rapidity dependence of the total counting rate in the three precision-chamber stations at nominal luminosity [15].*

Figure 9 shows the background environment of the ATLAS muon system. The impact of the background rate on the single tube spatial resolution was already discussed in detail in [6].

The background rates will not be constant. This effects the rt-relation in two different ways: Because of ions drifting back to the cathode space charge in the drift region builds up and causes a drift field change and a gain drop.

- Gain drop:
  Since the electric field on the wire becomes smaller in the presence of space charge, the gain drops. Measurements and simulations of the gain drop are described in [6]. We expect a gain drop of $G/G_0 \approx 0.87$ at a background rate of 1500 Hz/cm and $G_0 = 2 \cdot 10^4$. Figure 10 illustrates the reason for the systematic error. The average signal maximum for muons is $h \approx 150$ primary ionization electrons. Assuming a linear signal rising edge yields a shift of the threshold crossing time Δt_{thr} of ~ 0.4 ns (peaking time $t_p = 15$ ns, 20 electron threshold at a gain drop of $G/G_0 = 0.87$). With

a drift velocity $\sim 30\,\mu$m/ns we get an average systematic error of the predicted drift radius r of $\sim 12\,\mu$m. This value is almost independent of the drift gas. Thus the systematic error to the rt-relation due to gain drop is a very small effect and can be neglected even for bigger gain drops[8].

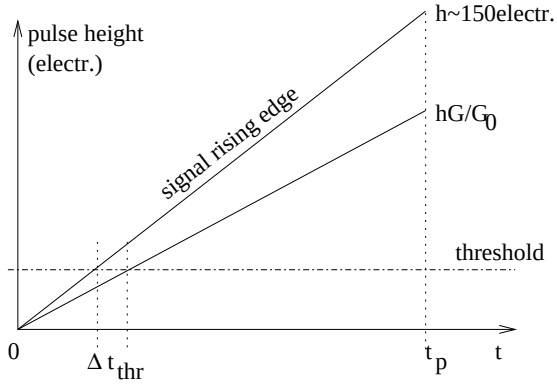

Figure 10: *At a given gain drop G/G_0 the threshold crossing time shifts to later times, consequently the drift radius is overestimated if the rt-relation without gain drop is used.*

- Drift field change:
  The ions which are drifting back from the wire to the cathode surface produce a charge density changing the drift field (see [6]). For non-linear gas mixtures like Ar/CO_2 this is the dominating systematic error to the rt-relation. Applying equation (7) the effect can be quantified and shows an error of $\delta r_F^{\text{r.m.s.}} = 120\,\mu$m for a rate difference of 1500 Hz/cm with Ar/CO_2 93/7 ($Ar/N_2/CH_4$ 91/4/5 gives only $18\,\mu$m). Figure 18 (a) shows that the systematic error to the rt-relation induced by high rate drift field changes is not linear with r, nevertheless the root mean square as described in equation (6) represents a very good figure of merit for the impact on the reconstructed muon momentum resolution.

In the appendix the derivation for a correction of the systematic error due to a drift field change is presented. The product of the background rate N_c, the gas gain G and the charge deposit Q can be extracted from the monitored chamber current ($I_{ch} = f(N_c G Q)$):

$$\delta r_F(t) = \frac{N_c G Q b^2 \log\frac{b}{a}}{8\pi\varepsilon_0 \mu V_0^2} \left[t r_0'(t) - r_0(t) + \frac{6\log\frac{b}{a}}{b^2} r_0'(t) \int_0^t \left(\frac{r_0'(t')}{r_0'(t)} - 1 \right) r_0(t')^2 \, \mathrm{d}t' \right], \qquad (7)$$

where μ is the ion mobility, V_0 the wire potential and $r_0'(t) = \frac{\partial r_0(t)}{\partial t}$ the first deviation of $r_0(t)$ (see appendix for a more detailed description).

Figure 11 shows the measurement, the simulation and the calculation of the systematic error $\delta r_F(t)$. The correction reduces the systematic error $\delta r_F^{\text{r.m.s.}}$ from $120\,\mu$m to $< 30\,\mu$m.

[8] The effect scales with $(\frac{G_0}{G} - 1)$.

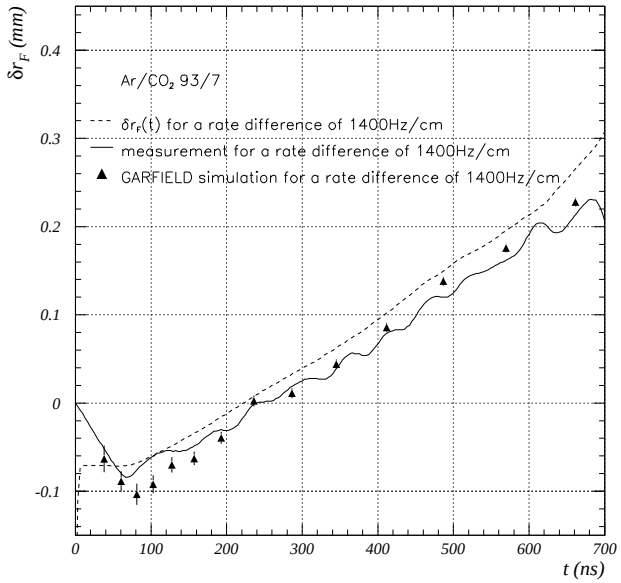

Figure 11: *The systematic error $\delta r_F(t)$ to the rt-relation due to rate variations $\delta r_F(t)$ as a function of the drift time t. The plot compares measurements with GARFIELD simulations and the calculation of $\delta r_F(t)$ according to equation (7).*

3.1.2 Temperature Effects

Various heat sources and sinks in the muon spectrometer will result in temperature gradients. Temperature differences in the muon spectrometer are estimated to be at the level of 3 K (see [15]).

The diurnal temperature variations in the cavern will be significantly smaller at the level of $\Delta T = \pm 1\,\mathrm{K}$.

Assuming constant pressure the following contributions have to be considered:

- Gas gain stability:
  Temperature related density variations induce gain variations. According to Diethorn's formula [10] ($\frac{\rho(T_0)}{\rho(T)} = \frac{T}{T_0}$, $T = T_0 + \Delta T$)

$$G(T) = \left[\frac{E(a)\rho(T_0)}{E_{min}(\rho(T_0))\rho(T)}\right]^{\frac{aE(a)}{\Delta V}\log 2} \quad \rightarrow \quad \frac{G(T)}{G(T_0)} = \left[\frac{T}{T_0}\right]^{\frac{V_0 \log 2}{\Delta V \log \frac{b}{a}}}, \tag{8}$$

  where $E(a)$ is the electric field on the wire surface and E_{min} and ΔV are the Diethorn parameters (see table 1 for Ar/CO_2 mixtures) a temperature change of $\Delta T = -5\,\mathrm{K}$ translates into a gain drop of $G(T)/G(T_0) = 0.9$. The impact of a gain drop has already been discussed in section 3.1.1. The systematic error to the rt-relation caused by this effect is negligible.

- Stability of the drift velocity:
  The drift velocity v_D is a function of $\frac{E}{\rho}$. Thus a change of the gas density will influence the drift time t at a given drift distance r. This systematic error to the rt-relation can be calculated (see equation (9) and the appendix). For Ar/CO_2 93/7 a temperature change of $\Delta T = 2\,\mathrm{K}$ results in an error of $\delta r_D^{\mathrm{r.m.s.}} = 27\,\mu\mathrm{m}$ (for $Ar/N_2/CH_4$ 91/4/5 $\delta r_D^{\mathrm{r.m.s.}} = 4\,\mu\mathrm{m}$).

In the ATLAS gas distribution the gas density will be controlled by keeping the ratio of $\frac{\text{pressure}}{\text{temperature}} \propto \rho$ constant (see also [13]). However, the gas density will perform small variations since the pressure equalizes in the gas volume. Nevertheless the control of the gas density in the gas distribution will further reduce temperature effects. We estimate the residual variations to be at the level of $|1 - \rho/\rho_0| < 0.4\,\%$ (see appendix), which cause a systematic error of $\delta r_D^{\mathrm{r.m.s.}} = 15\,\mu\mathrm{m}$.

In the appendix the impact of a gas density change on the rt-relation – e.g. as a consequence of temperature variations – is described in an analytical model. This model can predict the systematic error with high accuracy and hence makes a correction possible:

$$\delta r_D(t) = \left(\frac{\rho_0}{\rho} - 1\right)(r_0(t) - t \cdot r_0'(t)). \tag{9}$$

Figure 12 compares GARFIELD simulations and calculations of the systematic error due to large gas-density variations and shows excellent agreement.

Applying the density correction presented in equation (9) we can reduce the systematic error $\delta r_D^{\mathrm{r.m.s.}}$ to smaller than $10\,\mu\mathrm{m}$ provided the temperature of the gas is known with an accuracy of $0.2\,\%$.

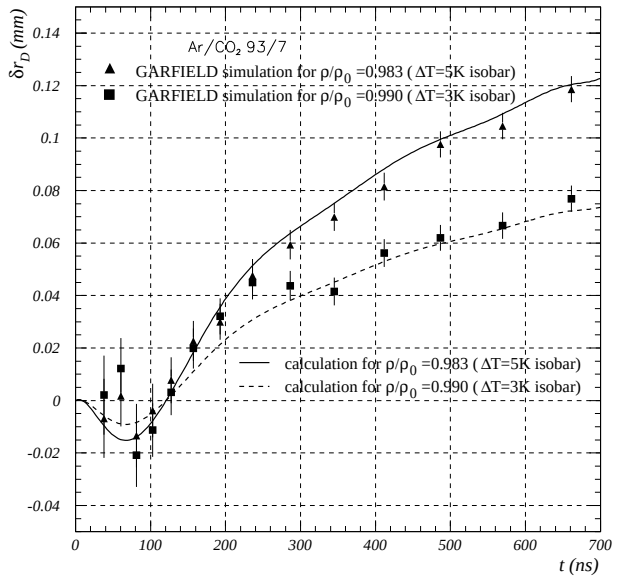

Figure 12: *The systematic error to the rt-relation $\delta r_D(t)$ due to density variation as a function of the drift time t. The plot compares GARFIELD simulations with the calculation of $\delta r_D(t)$ as described above and in the appendix.*

3.1.3 Gas Composition

The drift properties of Ar/CO_2 mixtures depend crucially on the exact CO_2 content. Table 2 points out the vast differences of the maximum drift time t_{max} for a change of the CO_2 content of only one percentage point. It is not the absolute value of the gas composition, but the stability in time, that will be crucial for the performance of our spectrometer. Another important aspect is the stability of the water content.

Figure 13 demonstrates the change of the drift properties in terms of a distortion of the rt-relation $\delta r_{gas\,comp}$. In order to restrict $\delta r^{\mathrm{r.m.s.}}_{gas\,comp}$ to a maximum of 40 μm, the absolute composition variation has to stay below 0.1 % absolute.

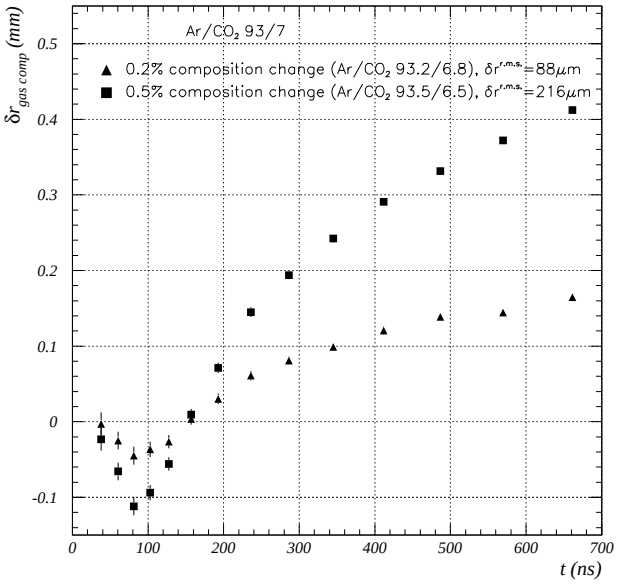

Figure 13: *Systematic error to the rt-relation due to changes of the gas composition. GARFIELD simulation, calculation of the gas properties with MAGBOLTZ.*

Because of the very small flow rate (1 volume exchange per 10 h) such variations in the gas composition will distribute very slowly over the whole muon system. Thus even with exact monitoring after the mixer it is very difficult to know the actual gas composition in the chambers. A correction for this effect is therefore hardly possible.

The water content of the MDT drift gas is not decided yet. Its value will be determined with regard to a maximum stability of the drift properties[9]. Figure 14 shows GARFIELD simulations of the systematic error due to variations of the water content. The nominal water content is 1000 ppm. As described in [14] the impact of water on the rt-relation is

[9]Usually the maximum drift time shows a minimum at a few thousand ppm depending on the drift gas. There the highest stability of the drift properties is guarantied (see [14]). This optimal water content has to be determined by measurements.

usually not very well predicted by GARFIELD. Nevertheless figure 14 gives us an estimate of the magnitude of the effect. If we estimate the stability of the water content to be 3 % the systematic error will be smaller than 10 μm. This value has to be confirmed by measurements.

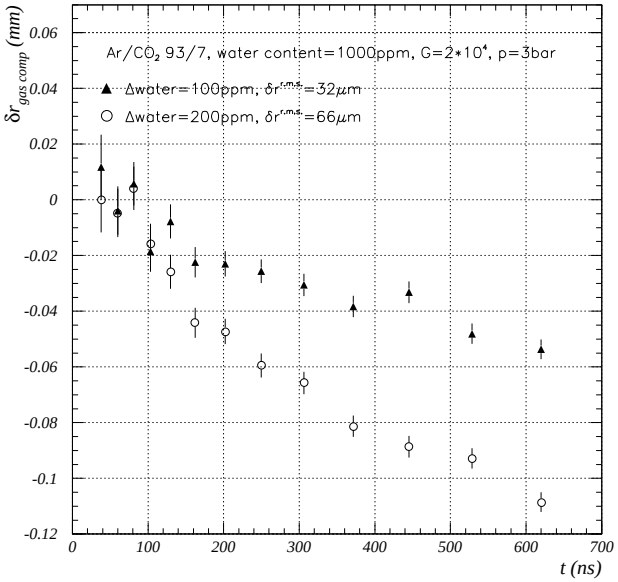

Figure 14: *Systematic error to the rt-relation due to changes of the water content. GARFIELD simulation, calculation of the gas properties with MAGBOLTZ.*

3.1.4 Concentricity of the Anode Wire

Temperature differences between MDT multilayers deform the chamber. The in-plane alignment will measure the fundamental mode of such deformations, but cannot prevent loss of concentricity of the anode wires relative to the tubes, which is required not to exceed 100 μm[10] [15]. Measurements on MDT prototypes, confirmed by finite-element calculations, show that gradients of $\Delta T = 3\,\mathrm{K}$ are tolerable for chambers with tube length below 3 m [16]. Such a non-concentricity of the wire translates into a rt-relation with two different branches, one for each side of the wire. Let be s the distance between the tube axis and the wire and the angle φ the polar angle, then the first order approximation (all

[10]I.e. the distance between the anode wire and the tube axis is not allowed to exceed 100 μm. Note that engineers define concentricity as the whole window of possible wire positions, according to this definition our tubes will have a concentricity of 200 μm.

terms with $\mathcal{O}[(s/b)^2]$ neglected) of the new drift field $|\vec{E}(r,\varphi)|$ is

$$|\vec{E}(r,\varphi)| = \frac{V_0}{r \log \frac{b}{a}} \left(1 + \frac{rs}{b^2} \cos\varphi\right) \tag{10}$$

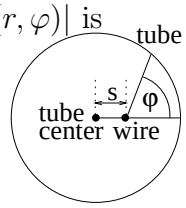

$\varphi = 0$ is fixed in the direction of the nearest distance between the non-concentric wire and the tube wall. Using equation (10) we can calculate the systematic error to the rt-relation δr_C as a function of s and φ – the derivation is shown in the appendix – ($r_0(t)$ is the rt-relation for $s = 0$):

$$\delta r_C(t) = 2\frac{s}{b^2} \cos(\varphi) r_0'(t) \int_0^t \left(\frac{r_0'(t')}{r_0'(t)} - 1\right) r_0(t')\, \mathrm{d}t'. \tag{11}$$

Figure 15 shows a measurement of a wire being 500 μm out of center and a calculation of $\delta r_C(t)$. For $s = 100\,\mu$m the r.m.s. of the difference between one branch and the rt-

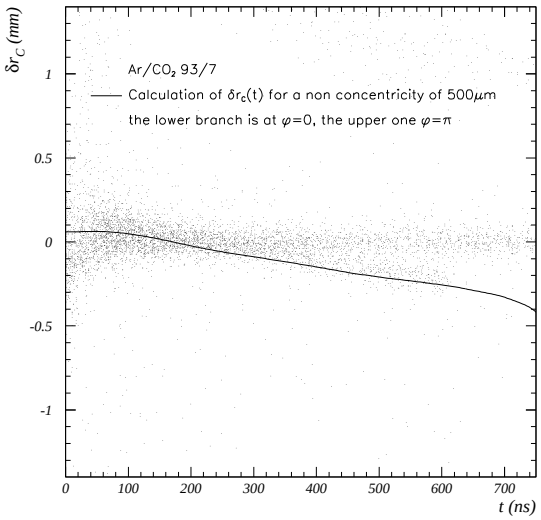

Figure 15: *Two branches of the rt-relation at a non-concentricity of 500 μm. The calculation of $\delta r_C(t)$ according to equation (11) fits very well to the measurement. The two branches are at $\varphi = 0$ and $\varphi = \pi$. The plot shows the residuals of single events (i.e. the position obtained with the branch of the rt-relation at $\varphi = \pi$ minus the position predicted by ODYSSEUS).*

relation for $s = 0$ is in the order of 15 μm for mixtures like Ar/CO_2. For linear gases such as $Ar/N_2/CH_4$ 91/4/5 the effect is negligible ($\delta r_C^{\text{r.m.s.}} = 2\,\mu$m). Autocalibration would deliver the mean between the two branches as rt-relation, the residual distribution will show non-Gaussian tails. However, the reconstructed muon momentum resolution stays almost unchanged (see section 3.3). Furthermore the effect will be even smaller in ATLAS because due to geometrical considerations the shortest line from the wire to the muon track will be most likely at $\varphi = \pm\frac{\pi}{2}$.

3.1.5 Differences of the Magnetic Field

The rt-relation depends on the magnetic field[11] B. Since the magnetic field will vary throughout the spectrometer autocalibration zones are restricted in its size. However, we have to expect differences in the magnetic field of $\Delta B \approx 100\,\mathrm{G}$ ($\Delta B/B \approx 2\,\%$) within one autocalibration zone. Hence we will obtain an average rt-relation within one zone, which will differ slightly from the local rt-relations.

Figure 16 presents GARFIELD simulations of the systematic error to the rt-relation due to differences of the magnetic field in one autocalibration zone. It shows a systematic error $\delta r_M^{\mathrm{r.m.s.}}$ of $8\,\mu$m for differences in the magnetic field of $2\,\%$. The systematic error due to differences of the magnetic field in one autocalibration zone is therefore a very small effect[12].

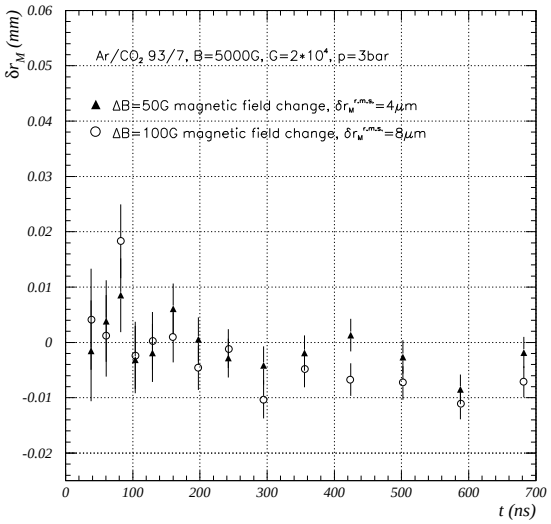

Figure 16: *Systematic Error δr_M due to differences in the magnetic field ($B = 0.5$ T parallel to the wire, $\Delta B = 50$ G and 100 G, $G = 2 \cdot 10^4$, $p = 3$ bar).*

3.1.6 Systematics of Autocalibration

The ATLAS Muon Spectrometer will assume the same Space-Time relation for certain areas of limited size. Within such areas the rt-relation will be obtained by autocalibration. The size of autocalibration zones will be determined by the necessary angular spread of the muon tracks ($\alpha_{tracks}^{\mathrm{r.m.s.}} \approx 2\,^\circ$), statistical considerations and the non-uniformity of the magnetic field.

[11] We consider only the influence of magnetic fields parallel to the wire (wire $\parallel z$) $\vec{B} = B_z \vec{e_z}$ like it will be to a first approximation in the ATLAS muon spectrometer.

[12] For larger Lorentz angles (see section 2.7) than the one of Ar/CO_2 93/7 the effect will increase slightly

The autocalibration method was developed and tested with testbeam measurements [17] and typically yields the rt-relation with an accuracy of $\delta^{\text{r.m.s.}}_{autocal} < 20\,\mu$m.

Compared to other sources of systematic errors to the rt-relation $\delta^{\text{r.m.s.}}_{autocal}$ is rather small, but it depends strongly on the angular spread of the muon tracks used.

Figure 17 shows measurements of the dependence of the systematic error $\delta^{\text{r.m.s.}}_{autocal}$ on the angular spread of the muon tracks $\alpha^{\text{r.m.s.}}_{tracks}$ (measurements with the Calypso MDT chamber [17]). It points out that for an angular spread of $\alpha^{\text{r.m.s.}}_{tracks} > 1.5\,^\circ$ the systematic error due to autocalibration $\delta^{\text{r.m.s.}}_{autocal}$ is smaller than $20\,\mu$m.

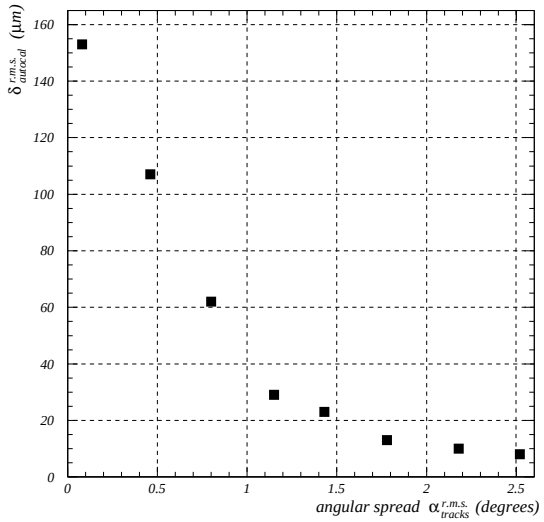

Figure 17: *The systematic error to the rt-relation due to autocalibration $\delta^{r.m.s.}_{autocal}$ as a function of the angular spread of the muon tracks $\alpha^{r.m.s.}_{tracks}$ (measurements from the H8 testbeam [17]).*

3.2 Systematic Errors with Linear and Non-Linear Drift Gases

Figure 18 summarizes the stability of the rt-relation for non-linear drift gases like Ar/CO_2 mixtures and linear gases such as $Ar/N_2/CH_4$ 91/4/5. Only the systematic errors due to a gain drop and due to autocalibration are gas independent. The plots are calculations performed according to the way introduced in the appendix. The magnitude of systematic errors is a direct measure for the linearity of a drift gas (the values for $\delta r^{\text{r.m.s.}}$ are listed in the plots and in table 3 for many different drift gases).

As expected we find big systematic errors to the rt-relation for non-linear gas mixtures, which might need a correction.

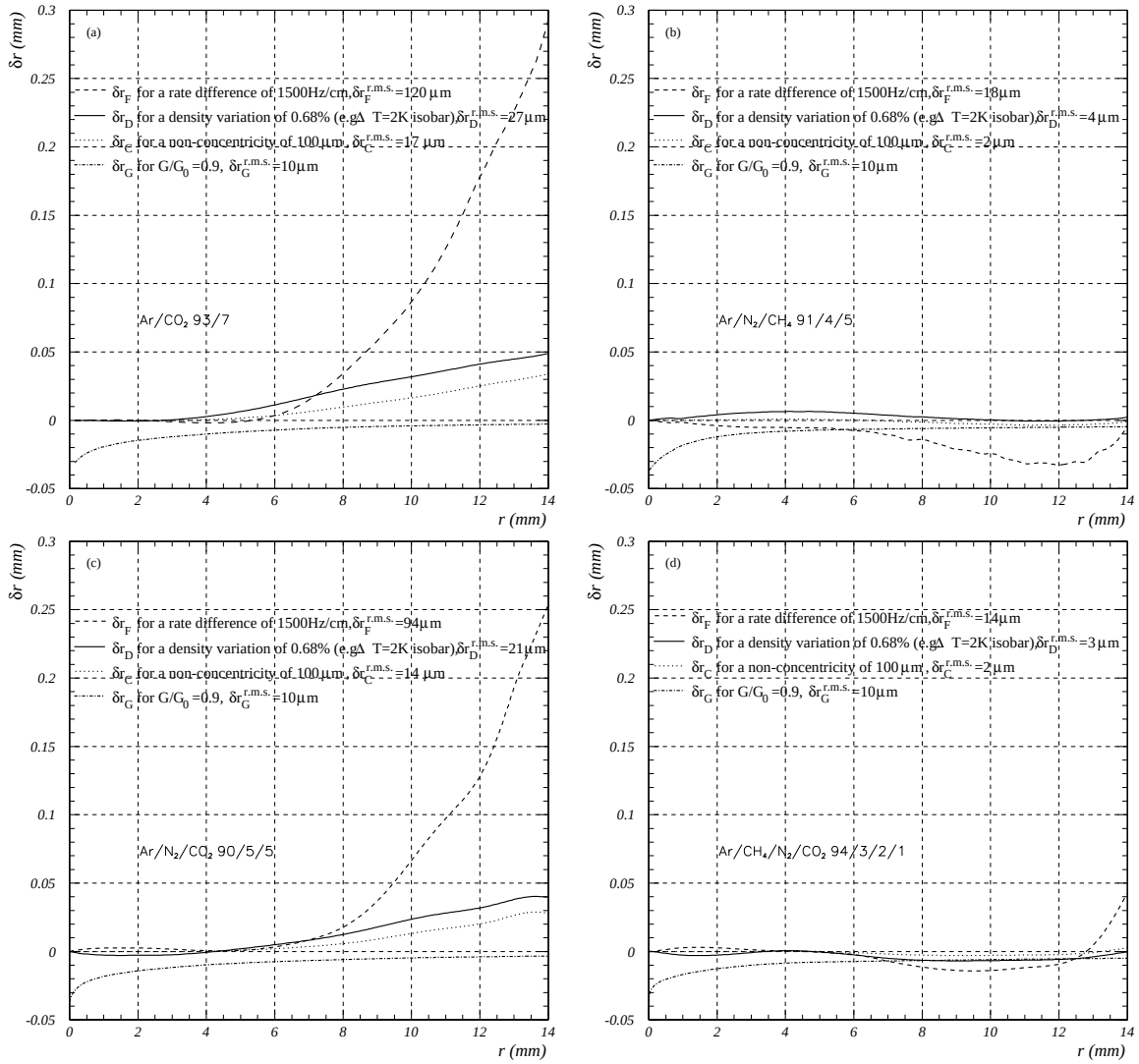

Figure 18: *Systematic errors to the rt-relations $\delta r(t) = r(t) - r_0(t)$ due to changes of the environmental parameters. The values for $\delta r^{r.m.s.}$ are listed in the plots.*

3.3 Impact of Systematic Errors to the Space-Time Relation on the Reconstructed Muon Momentum Resolution

In this chapter the systematic errors to the rt-relation have been discussed in detail up to now. In this chapter we want to study their influences on the reconstructed muon momentum resolution.

Figure 19 illustrates that the error on the reconstructed track position in one superlayer depends strongly on the angle and the position of the muon track. Therefore a correct simulation of the impact on the reconstructed muon momentum resolution has to involve the geometry of the whole spectrometer and the magnetic field. Such simulations have been performed with DICE/ATRECON. DICE [4] is a program based on GEANT calculating the output of all detector systems in ATLAS for real physics events using the exact geometry

gas mixture	$\delta r_F^{\text{r.m.s.}}$ (μm) $\Delta\text{Rate} =$ $= 1500\,\text{Hz/cm}$	$\delta r_D^{\text{r.m.s.}}$ (μm) $\rho/\rho_0 = 0.993$ ($\Delta T = 2\,\text{K}$ isobar)	$\delta r_C^{\text{r.m.s.}}$ (μm) $s = 100\,\mu\text{m}$	$\delta r_G^{\text{r.m.s.}}$ (μm) $G/G_0 = 0.9$	$\delta r_{autocal}^{\text{r.m.s.}}$ (μm)
$Ar/N_2/CH_4$ 91/4/5	18	4	2	10	< 20
$Ar/N_2/CO_2$ 90/5/5	94	21	14	10	< 20
$Ar/CH_4/N_2/CO_2$ 94/3/2/1	14	3	2	10	< 20
Ar/CO_2 90/10	123	28	18	10	< 20
Ar/CO_2 92/8	113	28	16	10	< 20
Ar/CO_2 93/7	120	27	17	10	< 20
Ar/CO_2 94/6	123	25	16	10	< 20

Table 3: *Values for the biggest expected errors $\delta r^{r.m.s.}$ to the rt-relation. The calculations have been done according to the method described in the appendix. The systematic errors due to variations of the gas composition and due to magnetic field differences have only been simulated for Ar/CO_2 93/7 and are therefore not included in the table (see sections 3.1.3 and 3.1.5).*

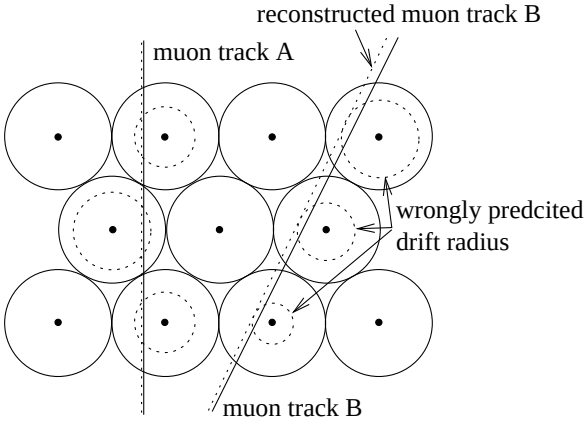

Figure 19: *The sketch shows the impact of systematic errors to the rt-relation on a reconstructed muon track in one super layer. Muon track A is reconstructed almost correctly despite the systematic error whereas the reconstructed muon track B shows a big deviation from the original position.*

of the detector. ATRECON is a program which reconstructs the momenta and energies of the particles by using the output of DICE.

In the simulations described here a perfect calibration of the magnetic field and a perfect chamber alignment was assumed

Figure 20 shows the results of the simulations. Only muons with a transverse momentum of $p_T = 1\,\text{TeV/c}$ were considered since errors in the position measurement have its biggest impact on the reconstruction of muon tracks with high momenta. For smaller muon momenta the resolution is dominated by multiple scattering.

Plot 20 (a) shows the contribution of systematic errors to the reconstructed muon mo-

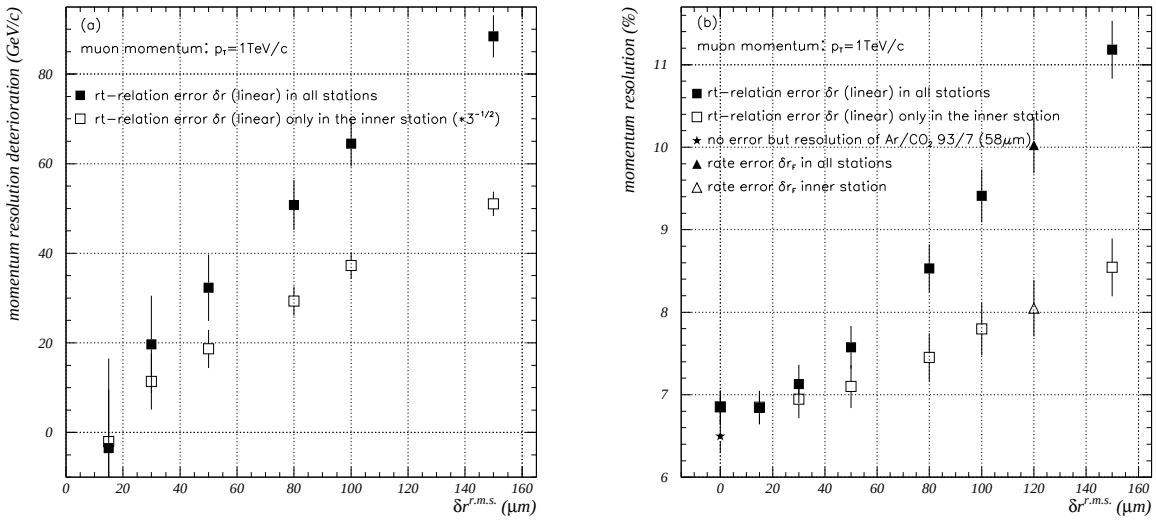

Figure 20: *DICE [4] simulations of the impact of a systematic error to the rt-relation on the reconstructed muon momentum resolution for muons with p_T = 1 TeV/c. Plot (a) shows the quadratic deterioration of the reconstructed muon momentum resolution with a distorted rt-relation in all chambers. The values for a systematic error only in the inner station have been obtained by scaling the deterioration with $\frac{1}{\sqrt{3}}$. Plot (b) illustrates the muon momentum resolution in %. The squares are simulations with a linear distortion ($\delta r(r) = \frac{\delta r^{r.m.s.}\sqrt{3}}{b} \cdot r$), the triangles show a simulation with a real distortion δr_F like shown in figure 18.*

mentum (quadratic difference to the value without systematic error). As expected a linear increase of the deterioration with $\delta r^{\text{r.m.s.}}$ can be seen. In order to obtain an estimate of the effect having a systematic error $\delta r^{\text{r.m.s.}}$ only in the inner station of the spectrometer, the contribution was scaled with $\frac{1}{\sqrt{3}}$.

Plot 20 (b) presents the relation between the reconstructed muon momentum and the systematic error $\delta r^{\text{r.m.s.}}$. It indicates that up to a systematic error of $\delta r^{\text{r.m.s.}} \leq 50\,\mu$m in all tubes of the detector the reconstructed momentum resolution stays almost unchanged ($\Delta p_T/p_T$ = 7–7.5 %). For bigger systematic errors the resolution degrades quickly. Considering a systematic error only in the inner muon station (e.g. systematic error due to rate effects) the deterioration of the resolution is less (white squares in the plot). The squares have been calculated using a linear distortion of the rt-relation ($\delta r(r) = \frac{\delta r^{\text{r.m.s.}}\sqrt{3}}{b} \cdot r$), whereas for the triangles a real systematic error $\delta r_F(r)$ like in figure 18 (a) was applied.

Since we expect much larger systematic errors $\delta r^{\text{r.m.s.}}$ than 50 μm for non-linear gas mixtures like Ar/CO_2, the appendix deals with possible corrections.

4 Conclusion

This note presents the operating point and systematic errors of the baseline gas Ar/CO_2 93/7. Furthermore it compares different drift gases in terms of resolution, and stability of the rt-relation.

Measurements and GARFIELD simulations agree on a resolution of $\sim 58\,\mu$m without background ($\sim 54\,\mu$m with time slewing correction) and $\sim 84\,\mu$m with a background rate of 1400 Hz/cm ($\sim 79\,\mu$m with time slewing correction) for the baseline gas Ar/CO_2 93/7 at a gas gain of $G_0 = 2 \cdot 10^4$. For higher gas gains the resolution without time slewing correction improves slightly with no background. But higher gain hardly improves the resolution with correction and rate effects become worse.

The afterpulsing rate was measured and was found to be 3 % (Ar/CO_2 93/7, $G = 2 \cdot 10^4$). Afterpulses themselves do not cause big problems (very small pulses) but are a sign of incomplete quenching properties of the considered drift gas.

baseline gas	Ar/CO_2 93/7
gas pressure p	3 bar
gas gain G_0	$2 \cdot 10^4$
operating voltage	3080 V
peaking time t_p	10–15 ns
noise σ_{noise}	$< 4\,e^-$
threshold	$5 \times$ noise ($\sim 20\,e^-$)
afterpulsing rate	3 %
maximum drift time	
no B-field $t_{max}^{0\,T}$	~ 700 ns
B-field of 0.5 T $t_{max}^{0.5\,T}$	~ 720 ns
Lorentz angle $\langle\Psi\rangle$	9.3 °
resolution $\bar{\sigma}$	
no rate	58 μm
rate of 1400 Hz/cm	84 μm
$\bar{\sigma}$ **time slew. corrected**	
no rate	54 μm
rate of 1400 Hz/cm	79 μm
maximum occupancy	
Rate = 300 kHz/tube	~ 15 %

Table 4: *Summary: Working point for the MDT's.*

effect	$\delta r^{\text{r.m.s.}}$ (μm)
background rate	
ΔRate = 1500 Hz/cm	120
with correction	< 30
gas density	
$\rho/\rho_0 = 0.993$	27
with correction	< 10
gas composition	
Δcomposition = 0.1 %	44
non-concentricity	
$s = 100\,\mu$m	17
gain drop	
$G/G_0 = 0.9$	10
B-field difference	
$\Delta B = 100$ G	8
autocalibration	< 20
total (quadratic sum)	
without correction	< 135
with correction	< 65

Table 5: *Summary: Systematic errors for the baseline gas.*

Table 4 summarizes the working point for our MDT system, in table 5 the systematic errors to the rt-relation (1-σ values) are listed. Adding all systematic errors (quadratic sum) results in $\delta r_{total}^{\text{r.m.s.}} < 135\,\mu$m respectively in $\delta r_{total}^{\text{r.m.s.}} < 65\,\mu$m if the corrections are applied. The systematic error with the corrections is dominated by the systematic error due to variations of the gas composition.

The different reasons for systematic errors to the rt-relation were discussed in detail. The

biggest effect is the background rate variation which will introduce a systematic error to the rt-relation of $\delta r_F^{\text{r.m.s.}} = 120\,\mu\text{m}$ ($\Delta\text{Rate} = 1500\,\text{Hz/cm}$ for the baseline mixture). Simulations of the impact of such systematic errors on the reconstructed muon momentum have been performed. They show that up to a systematic error of $\delta r^{\text{r.m.s.}} \leq 50\,\mu\text{m}$ the reconstructed momentum resolution stays almost unaffected ($\Delta p_T/p_T \approx 7$–$7.5\,\%$ for a $p_T = 1\,\text{TeV/c}$, perfect chamber alignment and magnetic field calibration assumed). For bigger systematic errors ($\delta r^{\text{r.m.s.}} > 50\,\mu\text{m}$) a rapid resolution deterioration was observed (see figure 20).

Two of the biggest systematic errors (i.e. the systematic error due to rate variations and due to density variations) can be predicted by analytical models. Corrections are introduced which can reduce the systematic error to a large extent (e.g. $\delta r_F^{\text{r.m.s.}} = 120\,\mu\text{m} \overset{\text{correction}}{\longrightarrow} \delta r_F^{\text{r.m.s.}} < 30\,\mu\text{m}$).

Measurements and GARFIELD simulations show very good agreement for a lot of the considered effects. The analytical model developed for corrections predicts the changes of the rt-relation with high accuracy.

In summary Ar/CO_2 has good aging properties, whereas linear gases with hydrocarbons tend to age. However, the non-linearity of Ar/CO_2 makes the rt-relationship much less stable with respect to changes in operating conditions. The effect of this has been quantified and is acceptable even in the regions of the spectrometer with highest background and even if the rate is five times what we expect.

Acknowledgement

We want to thank M. Deile for helping us during the testbeam period by setting up the beam telescope ODYSSEUS [8]. We are also very grateful towards N. Hessey for providing and maintaining the data acquisition software and for never hesitating to come to CERN during the weekends if there are problems.

Appendix

First Order Corrections

This chapter describes first order corrections to the rt-relation if the parameters, causing a systematic error are known. This will be the case for the gas density change, which can be calculated from the temperature measurements, and the background rate, which can be extracted from the current measurement.

In the following corrections to the rt-relation $r_0(t)$ at a gas density ρ_0 without background rate ($N_c = 0$) will be introduced. Thus the rt-relation becomes a function of $\frac{\rho}{\rho_0}$ and $N_c \cdot G$ where N_c is the background rate per unit length and G the gas gain:

$$\begin{aligned} r(t, \frac{\rho}{\rho_0}, N_c \cdot G) &= r_0(t) + \delta r_D(t, \frac{\rho}{\rho_0}) + \delta r_F(t, N_c \cdot G) = \\ &= r_0(t) + \left(\frac{\rho_0}{\rho} - 1\right) \mathcal{D}_{corr}(t) + \nu(N_c \cdot G)\mathcal{F}_{corr}(t). \end{aligned} \tag{12}$$

The dimensionless parameter ν which contains the background rate N_c, the gas gain G and the average charge deposit Q and the two $r_0(t)$-dependent functions $\mathcal{D}_{corr}(t)$ and $\mathcal{F}_{corr}(t)$ will be discussed later. Because of

$$r(t) = \int_0^t v(t')\ \mathrm{d}t' \quad \rightarrow \quad r_0(t) + \delta r(t) = \int_0^t v_0(t')\ \mathrm{d}t' + \int_0^t \delta v(t')\ \mathrm{d}t' \tag{13}$$

we obtain

$$\delta r(t) = \int_0^t \delta v(t')\ \mathrm{d}t' = \int_0^t (\overbrace{v_0'(t')}^{r_0''(t')} \Delta t(t') + \mathcal{O}[\Delta t(t')^2])\ \mathrm{d}t', \tag{14}$$

where $\Delta t(t)$ is defined by

$$\mathcal{E}_0(r_0(t' + \Delta t(t'))) \equiv \mathcal{E}_{new}(r(t')). \tag{15}$$

In equation (15) $\mathcal{E}_0(r)$ stands for $\frac{E_0(r)}{\rho_0}$, where $E_0(r)$ is the drift field without background rate and ρ_0 the gas density when $r_0(t)$ was autocalibrated. $\mathcal{E}_{new}(r)$ is the new drift field divided by the new gas density $\frac{E_{new}(r)}{\rho}$. The drift velocity $v(t)$ is a function of $\frac{E}{\rho}$ and therefore of $\mathcal{E}$, therefore $v_0'(t')\Delta t(t')$ represents the first order correction of the drift velocity (see figure 21).

In the following we want to separate the two effects, thus either the drift field changes ($E_0 \rightarrow E_{new}$ and $r(t) = r_0(t) + \delta r_F(t)$) or the gas density changes ($\rho_0 \rightarrow \rho$ and $r(t) = r_0(t) + \delta r_D(t)$). Taylor expansion of the left side of equation (15) yields (terms with $\mathcal{O}[\Delta t(t')^2]$ or higher are neglected):

$$\begin{aligned} \mathcal{E}_0(r_0(t')) + \frac{\partial \mathcal{E}_0(r_0(t'))}{\partial t'} \Delta t(t') &= \mathcal{E}_{new}(r(t')), \\ -\frac{V_0 r_0'(t')}{\rho_0 r_0(t')^2 \log \frac{b}{a}} \Delta t(t') &= \mathcal{E}_{new}(r(t')) - \mathcal{E}_0(r_0(t')), \end{aligned} \tag{16}$$

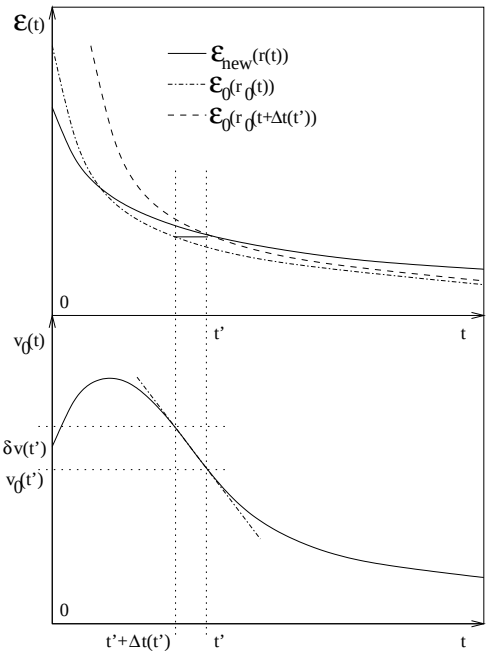

Figure 21: *Sketch illustrating equation (15). $v_0'(t')\Delta t(t')$ is the necessary correction to the drift velocity ($\delta v(t')$) for the time t'.*

where $\mathcal{E}_0(r) = \frac{V_0}{\rho_0 r \log \frac{b}{a}}$ was used (a is the wire radius and b is the inner tube radius, here $a = 25\,\mu$m and $b = 1.46\,$cm). In the following the calculation of $\mathcal{E}_{new}(r(t')) - \mathcal{E}_0(r_0(t'))$ for the different effects will be discussed.

Gas Density Correction $\delta r_D(t)$

The gas density will be controlled in the gas distribution. Still, different gas temperatures in the gas volume will cause density variations. These density variations will be rather difficult to predict but in principle we can calculate the gas density ρ in a chamber part by using the monitored temperature T on the chamber, the gas density ρ_{rack} and the temperature T_{rack} in the gas distribution and take advantage of the fact, that the pressure will equalize in the gas volume (the gravitational pressure drop[13] is $\xi = 0.53\,$mbar/m).

We can consider our drift gas to obey the ideal gas equation:

$$\rho \cdot R \cdot T = p \quad \rightarrow \quad \rho = \frac{\rho_{rack} R T_{rack} - \Delta h \xi}{RT}, \tag{17}$$

where ρ is the gas density in the considered chamber, R the gas constant (e.g. $R_{\mathrm{Ar}} = 208\,\mathrm{J\,kg^{-1}K^{-1}}$, $R_{\mathrm{CO_2}} = 188\,\mathrm{J\,kg^{-1}K^{-1}}$), T the gas temperature in the chamber, Δh the altitude difference between the gas distribution and the considered chamber and p the gas pressure. Equation (17) yields for $\Delta h = 5\,$m and a difference between the temperature variation in the chamber (ΔT) and the temperature variation in the gas distribution[14]

[13]Only chambers in approximately the same altitude will be connected to reduce pressure differences induced by gravitation.

[14]Both (ΔT and ΔT_{rack}) with respect to the temperature during autocalibration.

(ΔT_{rack}) of $\Delta T - \Delta T_{rack} = 1\,\mathrm{K}$ a density decrease of $\rho/\rho_0 = 0.9957$.

As described in section 3.1.2 the gas density ρ_{rack} will be kept constant.

With equation (17) we obtain by applying Taylor expansion ($r(t) = r_0(t) + \delta r_D(t)$, $\delta r_D(t) \ll r_0(t) \quad \forall\, t$):

$$\begin{aligned} \mathcal{E}_{new}(r(t)) - \mathcal{E}_0(r_0(t)) &= \frac{\rho_0}{\rho}\frac{V_0}{\rho_0 r_0(t)\log\frac{b}{a}}\left(1 - \frac{\delta r_D(t)}{r_0(t)}\right) - \frac{V_0}{\rho_0 r_0(t)\log\frac{b}{a}} = \\ &= \frac{V_0}{\rho_0 r_0(t)\log\frac{b}{a}}\left(\frac{\rho_0}{\rho} - 1 - \frac{\rho_0}{\rho}\frac{\delta r_D(t)}{r_0(t)}\right) \end{aligned} \tag{18}$$

Using equations (16) and (14) we get:

$$\delta r_D(t) = \int_0^t \frac{r_0''(t')}{r_0'(t')}\left[\left(\frac{\rho_0}{\rho} - 1\right) r_0(t') + \frac{\rho_0}{\rho}\delta r_D(t')\right]\,\mathrm{d}t'. \tag{19}$$

Differentiation on both sides yields a differential equation with the solution

$$\delta r_D(t) = -\left(\frac{\rho_0}{\rho} - 1\right) r_0'(t)^{\frac{\rho_0}{\rho}} \int_0^t \frac{r_0''(t')}{r_0'(t')^{\left(1+\frac{\rho_0}{\rho}\right)}} r_0'(t')\,\mathrm{d}t'. \tag{20}$$

For real rt-relations ($r_0'(t)$ varies less than a factor 5 over the whole drift time t) and density changes less then 1 % ($|\frac{\rho_0}{\rho} - 1| < 0.01$, this corresponds to an isobar temperature change of $|\Delta T| < 3\,\mathrm{K}$) we can regard $r_0'(t)^{-\left(\frac{\rho_0}{\rho}-1\right)}$ as constant, put it out of the integral and cancel it down (error less than 2 %):

$$\delta r_D(t) = -\left(\frac{\rho_0}{\rho} - 1\right) r_0'(t) \int_0^t \frac{r_0''(t')}{r_0'(t')^2} r_0'(t')\,\mathrm{d}t'. \tag{21}$$

The remaining integral can be solved:

$$\boxed{\delta r_D(t) = \left(\frac{\rho_0}{\rho} - 1\right)\left(r_0(t) - t \cdot r_0'(t)\right) = \left(\frac{\rho_0}{\rho} - 1\right)\mathcal{D}_{corr}(t).} \tag{22}$$

The obtained correction was compared to GARFIELD[15] simulations and shows excellent agreement (see figure 12).

Rate Correction $\delta r_F(t)$

As described in section 3.1.1 the ATLAS muon system will have to cope with rate differences of up to 1500 Hz/cm. Section 3.3 shows the big impact of systematic errors to the rt-relation on the reconstructed muon momentum resolution.

[15] GARFIELD [1] is interfaced to MAGBOLTZ [3] which calculates the drift properties of gas mixtures at given temperatures.

The rate correction $\delta r_F(t)$ is a function of the product $N_c \cdot G$, where N_c is the background count rate per unit length along the wire and G the effective gas gain including the gain drop. Furthermore the average charge deposit per background event Q has to be known[16]. The value of the product $N_c \cdot G \cdot Q$ can be derived from the current I_{ch} in the operating chamber. This current I_{ch} will be monitored.

$$N_c \cdot G \cdot Q = \frac{I_{ch}}{\mathcal{L}_{ch}}, \tag{23}$$

where $\mathcal{L}_{ch}$ is the total tube length of the considered chamber. In equation (23) a homogeneous irradiation of the chamber was assumed.

In [6] a first order approximation of the field change as a consequence of space charge was introduced. Using the dimensionless parameter ν

$$\nu \equiv \frac{N_c G Q b^2 \log\frac{b}{a}}{8\pi\varepsilon_0 \mu V_0^2} = \frac{I_{ch} b^2 \log\frac{b}{a}}{8\pi\varepsilon_0 \mu \mathcal{L}_{ch} V_0^2}, \tag{24}$$

where μ is the ion mobility (e.g. $\mu_{\mathrm{Ar}^+ \text{ in } \mathrm{Ar}}(1\,\mathrm{bar}) = 1.535\,\mathrm{cm^2 V^{-1} s^{-1}}$ [19]) and a and b the wire and tube radius, we get:

$$\mathcal{E}(r(t)) = \frac{V_0}{\rho_0 r(t) \log\frac{b}{a}}(1-\nu) + \frac{2\nu V_0}{\rho_0 b^2}\, r(t). \tag{25}$$

Applying Taylor expansion ($r(t) = r_0(t) + \delta r_D(t)$, $\delta r_D(t) \ll r_0(t) \quad \forall\ t$) and using equation (16) we obtain

$$\Delta t(t) = \frac{1}{r_0'(t)} \left[\nu r_0(t) - \frac{2\nu \log\frac{b}{a}}{b^2} r_0(t)^3 + \delta r_F(t) \left(1 - \nu - \frac{2\nu \log\frac{b}{a}}{b^2} r_0(t)^2 \right) \right]. \tag{26}$$

Inserting in equation (14) and differentiating on both sides yields a differential equation

$$\delta r_F(t) \frac{r_0''(t)}{r_0'(t)} \left(1 - \nu - \frac{2\nu \log\frac{b}{a}}{b^2} r_0(t)^2 \right) - \frac{\partial \delta r_F(t)}{\partial t} = \frac{r_0''(t)}{r_0'(t)} \left(\frac{2\nu \log\frac{b}{a}}{b^2} r_0(t)^3 - \nu r_0(t) \right) \tag{27}$$

with the solution

$$\delta r_F(t) = \nu r_0'(t)^{(1-\nu)} e^{-g(t)} \int_0^t e^{g(t')} \frac{r_0''(t')}{r_0'(t')^{(2-\nu)}} \left(r_0(t') - \frac{2\log\frac{b}{a}}{b^2} r_0(t')^3 \right) \mathrm{d}t'. \tag{28}$$

The function $g(t)$ in equation (28) is defined as

$$g(t) \equiv \frac{2\nu \log\frac{b}{a}}{b^2} \int_0^t \frac{r_0''(t')}{r_0'(t')} r_0(t')^2 \,\mathrm{d}t' \tag{29}$$

and has values for mixtures like $\mathrm{Ar/CO_2}$ between $g(0) \approx 10^{-4}$ and $g(t_{max}) \approx 6 \cdot 10^{-2}$, and even smaller values for less non-linear gas mixtures. Hence the exponential function in

[16] Simulations determined the average energy deposit of a background photon to be $\sim 36\,\mathrm{keV}$ at a magnetic field of 0.6 T [18]

the integral can be regarded as constant, be written out of the integral and be cancelled down (error less than 6 %). The same applies for the $r_0'(t)^{-\nu}$-terms (even for the highest considered background rates ν is smaller than 10^{-2} and $r_0'(t)$ usually varies less than a factor 5 over the whole drift time $t \rightarrow$ error less than 2 %). Simplifying the integrals leads to

$$\boxed{\delta r_F(t) = \nu \left[t r_0'(t) - r_0(t) + \frac{6 \log \frac{b}{a}}{b^2} r_0'(t) \int_0^t \left(\frac{r_0'(t')}{r_0'(t)} - 1 \right) r_0(t')^2 \, \mathrm{d}t' \right] = \nu \mathcal{F}_{corr}(t).} \quad (30)$$

Figure 11 compares measurements with GARFIELD simulations and the calculation of $\delta r_F(t)$ according to equation (30) and shows a good agreement. The correction reduces $\delta r_F^{\text{r.m.s.}}$ from 120 μm to $< 30\,\mu$m. Note, that Equation (30) overestimates the rate effect at high rates (see Figure 11) since a first order approximation for the field change was used in Equation (25), which overestimates the rate effect for high rates at big radii.

Non-Concentricity Correction $\delta r_C(t)$

In this section we want to derive equation (11). As a starting point we want to use equation (10), which was obtained by calculating the electric field for a small deviation s of the wire out of the tube center by means of mirror charges[17]: The line charge on the wire was found to be

$$\gamma = \frac{2\pi\varepsilon_0 V_0}{\log \frac{b^2 - s^2}{ab}} = \frac{2\pi\varepsilon_0 V_0}{\log \frac{b}{a}} \cdot \left[1 + \frac{s^2}{b^2 \log \frac{b}{a}} + \mathcal{O}[(s/b)^4] \right]. \quad (31)$$

Writing down the whole expression for the electric field

$$\vec{E}(x,y) = \frac{V_0}{\log \frac{b^2 - s^2}{ab}} \cdot \left[\frac{\begin{pmatrix} x - s \\ y \end{pmatrix}}{(x-s)^2 + y^2} - \frac{\begin{pmatrix} x - \frac{b^2}{s} \\ y \end{pmatrix}}{(x - \frac{b^2}{s})^2 + y^2} \right], \quad (32)$$

transforming it into polar coordinates ($x = r\cos\varphi + s$ and $y = r\sin\varphi$) and performing a Taylor expansion for $s \ll b$ leads to

$$|\vec{E}(r,\varphi)| = \frac{V_0}{r \log \frac{b}{a}} \left(1 + \frac{rs}{b^2} \cos\varphi + \mathcal{O}[(s/b)^2] \right), \quad (33)$$

which is identical with equation (10). Following the way which was used for the other corrections we start with

$$\mathcal{E}_{new}(r(t)) - \mathcal{E}_0(r_0(t)) = \frac{V_0}{\rho_0 \log \frac{b}{a}} \left(\frac{s}{b^2} \cos\varphi - \frac{\delta r_C}{r_0(t)^2} \right), \quad (34)$$

[17] The line charge γ at the distance s from the tube center produces a mirror line charge $\tilde{\gamma} = -\gamma$ at the distance $\frac{b^2}{s}$ from the tube center, which lies outside the tube.

where Taylor expansion was used ($r(t) = r_0(t) + \delta r_C(t)$, $\delta r_C(t) \ll r_0(t) \quad \forall\, t \rightarrow \frac{1}{r_0(t)+\delta r_C(t)} = \frac{1}{r_0(t)} - \frac{\delta r_C(t)}{r_0(t)^2} + \mathcal{O}[\delta r_C(t)^2]$). Using equation (14) and differentiating on both sides yields a differential equation

$$\frac{\partial \delta r_C(t)}{\partial t} - \frac{r_0''(t)}{r_0'(t)} \delta r_C(t) = -\frac{r_0''(t)}{r_0'(t)} \cdot \frac{s r_0(t)^2}{b^2} \cos\varphi, \tag{35}$$

with the solution already shown in equation (11)

$$\boxed{\delta r_C(t) = -\frac{s}{b^2} \cos(\varphi) r_0'(t) \int_0^t \frac{r_0''(t')}{r_0'(t')^2} r_0(t')^2 \, \mathrm{d}t' = 2\frac{s}{b^2} \cos(\varphi) r_0'(t) \int_0^t \left(\frac{r_0'(t')}{r_0'(t)} - 1 \right) r_0(t') \, \mathrm{d}t'.} \tag{36}$$

Figure 15 compares the measurement of the two branches of the rt-relation for $\varphi = 0$ and $\varphi = \pi$ with the prediction of the effect using equation (36) and shows very good agreement.

References

[1] R. Veenhof, GARFIELD: Simulation of gaseous detectors, CERN, write-up: `http://wwwinfo.cern.ch/writeup/garfield`

[2] I. Smirnov, HEED, program to compute energy loss of fast particles in gases, CERN.

[3] S. Biagi, MAGBOLTZ, program to compute gas transport parameters, CERN.

[4] A. Artamonov et al. A.: DICE-95, ATL-SOFT-95-014

[5] The ATLAS Muon Detector Physics Group: Criteria for the Choice of the MDT Operating Point, ATLAS Internal Note MUON-NO-098 (1995).

[6] M. Aleksa, M. Deile, N.P. Hessey, W. Riegler: MDT Performance in a High Rate Background Environment, ATLAS Internal Note MUON-NO-258 (1998).

[7] Common base preamplifier IO354-2 and shaping amplifier IO532-01, Instrumentation Division, Brookhaven National Laboratory, Upton, New York, 1973.

[8] M. Deile, J. Dubbert, N.P. Hessey, A. Staude: ODYSSEUS – a Silicon Telescope for Test Beam Experiments, System Description and User Manual for the Data Analysis, LMU Munich 1998, available on the WWW-page: `http://www.etp.physik.uni-muenchen.de/atlas/testbeam.html`

[9] M. Deile et al.: Test Beam Studies of the Gas Mixtures ... for Drift Tubes, ATLAS Muon Note 122, 1996.

[10] W. Diethorn: A methane proportional counter system for natural radiocarbon measurements, USAEC Report NY06628 (1956).

[11] M. Aleksa, W. Riegler: Bipolar versus Unipolar Shaping of MDT Signals, ATLAS Muon Note, CERN 1998

[12] C.M. Ma et al., MIT Technical Report 129 (1982)

[13] M. Deile, N.P. Hessey: Density Control of MDT Gas, ATLAS Internal Note MUON-NO-203 (1997).

[14] S. Kircher et al., Influence of aqueous vapour on the drift properties of MDT gases, ATLAS Internal Note MUON-NO-214 (1997).

[15] ATLAS Muon Collaboration: Technical Design Report, CERN/LHCC 97-22, June 1997, available on the WWW-page: `http://atlasinfo.cern.ch/Atlas/GROUPS/MUON/TDR/Web/TDR.html`

[16] C.W. Daly et al.: ATLAS Internal Note MUON-NO-144 (1997).

[17] P. Creti et al.: Testbeam results from the Calypso MDT chamber, ATLAS Muon Note 196, CERN 1997.

[18] I.R. Boyko, G.A. Chelkov, V. Dodonov, M.A. Ignatenko, M. Nikolenko, V. Zhuravlev: MDT Gamma Response, ATLAS Muon Note 194, CERN 1997

[19] E.W. McDaniel and E.A. Mason: The Mobility and Diffusion of Ions in Gases (Wiley, New York 1973)